

## INTERNAL ELECTRIC FIELD PROFILE OF a-Si:H AND a-SiGe:H SOLAR CELLS

XINHUA GENG<sup>1\*</sup>, LEI WU,<sup>1</sup> KENT PRICE,<sup>1</sup> XUNMING DENG<sup>2</sup>, QI WANG<sup>3</sup>, AND DAXING HAN<sup>1</sup>

1. Dept of Phys & Astronomy, Univ of North Carolina at Chapel Hill, Chapel Hill, NC 27599-3255, USA. \*Permanent address: Institute of Photoelectronics, Nankai Univ. Tianjing, China.
2. Energy Conversion Devices, Inc., 1675 West Maple Rd. Troy, Michigan 48084, USA
3. National Renewable Energy Laboratory, Golden, CO 80401, USA.

### ABSTRACT

By using the transient-null-current method, we have measured the internal electric field profiles  $E_i(x)$  near the  $p/i$  interface for two groups of solar cells: (a) a-Si:H  $p-i-n$  solar cells with varied  $i$ -layer thicknesses, and (b) a-SiGe:H cells with varied Ge content. When using an exponential function of  $E_i(x)$  to fit the experimental results, we obtained the field strength at the  $p/i$  interface  $E_0$ , the screening length  $L_0$ , and the density of defect states  $N_d$  in the  $i$ -layer. The thinner the  $i$ -layer, the stronger the field strength obtained. For  $i$ -layer thickness increasing from 0.1 to 0.5  $\mu\text{m}$ , the field strength  $E_0$  decreases from  $1.15 \times 10^5$  to  $2.0 \times 10^4$  V/cm;  $L_0$  decreases from 0.89 to 0.14  $\mu\text{m}$ ; and  $N_d$  is  $3\text{--}4 \times 10^{16}$  ( $\text{cm}^3\text{eV}$ )<sup>-1</sup>. For the a-SiGe:H cells, as the Ge content increases from 40 to 55 %,  $E_0$  increases from  $9.3 \times 10^4$  to  $1.2 \times 10^5$  V/cm. The correlation of the internal electric field parameters with the cell's performance is discussed.

### INTRODUCTION

For high efficiency amorphous silicon solar cells, dual- or triple-junction tandem structures are used.[1] The charge collection of the a-Si:H and a-SiGe:H cells are crucial for the short- and long wave length performance, respectively. Since the charge collection process in a-Si:H based solar cells depends upon field-assisted drift in the internal-electric-field, the knowledge of the electric-field profile is important for device design. One needs to know how the electric field distribution changes with  $i$ -layer thickness and the Ge content, and how this affects the  $V_{oc}$  and the quantum efficiency wavelength dependence. By using computer simulation, the relation of the electric field distribution with  $V_{oc}$  of a-Si based alloy  $p-i-n$  cells under steady state light illumination has been studied by Hack et al. [2] and Fonish et al. [3]. The results show that the electric field  $E(x)$  decays exponentially from the junction interfaces. The value and the decay rates depend on the space charge density and the carrier's mobility. Assuming the internal field is screened by a constant midgap state,  $N_d$ , and neglecting the free carriers contribution, from the Poisson equation one obtains the field distribution from the junction interfaces decays exponentially. Here we consider the field decay from  $p/i$  interface as follows:

$$E_i(x) = E_0 e^{-\beta x} \quad (1)$$

where  $E_0$  is the field strength at the  $p/i$  junction interface, and  $x$  is the distance from the interface in the  $i$  layer.  $\beta$  is defined as

$$\beta = 1/L_0 = \sqrt{qN_d/\epsilon} \quad (2)$$

where  $L_0$  is the screening length, the electron charge  $q=1.6 \times 10^{-19}$  coulomb, and the dielectric constant  $\epsilon=10^{-12}$  F/cm. On the other hand, few experimental results have been published.[4-7] Among them the transient-null-current method is an attractive technique because the experimental knowledge of  $E_i(x)$  can be obtained in a real  $p-i-n$  cell structure. In this paper we

present the experimental results of  $E_i(x)$  on a-Si:H and a-SiGe:H solar cells with varied i-layer thickness and Ge content by using the transient null-current method. As in the previous works of the null-current technique in a-Si solar cells, [4,7] the transient photocurrent  $j_{pc}$  generated by a low-intensity pulsed laser was tuned to zero by the forward-bias voltages as

$$j_{pc} \propto \int_0^L [E_i(x) - V_a(\lambda)/L] e^{-\alpha(\lambda)x} dx = 0 \quad (3)$$

where  $V_a(\lambda)$  is the applied voltage at null-current condition as a function of wavelength  $\lambda$ ,  $L$  is the i-layer thickness, and  $\alpha(\lambda)$  is the absorption coefficient. Inserting Eq. (1) into Eq. (3) one obtains

$$\int_0^L [(E_0 e^{-\beta x}) - V_a(\lambda)/L] e^{-\alpha(\lambda)x} dx = 0. \quad (4)$$

With a specific absorption coefficient  $\alpha(\lambda)$ , one finds the fitting parameters to the experimental data of  $V_a(\lambda)$  by solving the integral. Finally, the best-fit parameters  $E_0$ ,  $L_0$ , and  $N_d$  will be obtained, and these parameters are used to calculate the electric field near the p/i interface using equation (1).

## SAMPLE AND EXPERIMENT

Samples were made at Energy Conversion Devices (ECD) by plasma-enhanced CVD. Several structures were studied i.e. a-Si:H stainless-steel/n-i-p/ITO cells with varied i-layer thickness, and a-SiGe:H ss/n-i-p/ITO cells with varied Ge content. The sample's parameters are listed in Tables I and II, respectively. A pulsed  $N_2$  laser that pumped a dye laser in a wavelength range of 380-640 nm was used for the photo excitation. Neutral density filters were used to adjust the incident light flux. The pulse light was illuminated through the semi-transparent ITO and wide-band gap p-layer on to the intrinsic layer. A 150 MHz pulse generator with  $1 \times 10^{-11}$  sec resolution was used to apply a positive voltage pulse  $V_a$ . The measurements were made at room temperature. The detailed experimental conditions can be found elsewhere. [4,7]

## RESULTS

### Dependence of the electric field profile on i-layer thickness

Table I. ss/n-i-p/TCO solar cell performance and the fitting parameters of  $E_i(x)$

Sample ID	i-layer thickness ( $\mu\text{m}$ )	$V_{oc}$ (V)	$J_{sc}$ ( $\text{mA}/\text{cm}^2$ )	FF	$P_{max}$ ( $\text{mW}/\text{cm}^2$ )	$E_0$ (V/cm)	$\beta$ ( $\mu\text{m}$ ) <sup>-1</sup>	$L_0$ ( $\mu\text{m}$ )	$N_d$ ( $\text{cm}^{-3}\text{eV}$ ) <sup>-1</sup>
LL843	0.1	0.945	8.67	0.70	5.73	$1.15 \times 10^5$	1.12	0.89	–
LL794	0.2	0.949	11.29	0.66	7.05	$5.32 \times 10^4$	2.57	0.37	–
LL795	0.4	0.947	13.23	0.57	7.11	$2.7 \times 10^4$	8.00	0.13	$4 \times 10^{16}$
LL793	0.5	0.947	13.25	0.55	6.93	$2.0 \times 10^4$	7.00	0.14	$3 \times 10^{16}$

Figure 1(a) shows the applied voltage  $V_a(\lambda)$  as a function of the laser wavelength  $\lambda$  for the a-Si:H cells with varied i-layer thickness. The dashed lines are the fitting curves according to Eq. (4) by using the  $E_i(x)$  functions shown in Fig. 1(b).  $E_i(x)$  is only shown near the p/i interface

since that is where it is most valid. One can see that  $V_a$  decreases drastically when  $\lambda > 475$  nm in 0.1 and 0.2- $\mu\text{m}$ -thin cells. We believe this is due to the hole transport evolving when the photo-excited carriers were generated through the thin *i*-layer as discussed below.  $V_a$  decreases smoothly in 0.4 and 0.5- $\mu\text{m}$ -thick cells. The best-fit parameters are listed in Table I. The density of the midgap states  $N_d$  is calculated according to Eq. (2). The values of  $N_d$  in thin cells can not be simply deduced from Eq. (2), because of the strong influence on  $E_i(x)$  from the *n*/*i* junction.

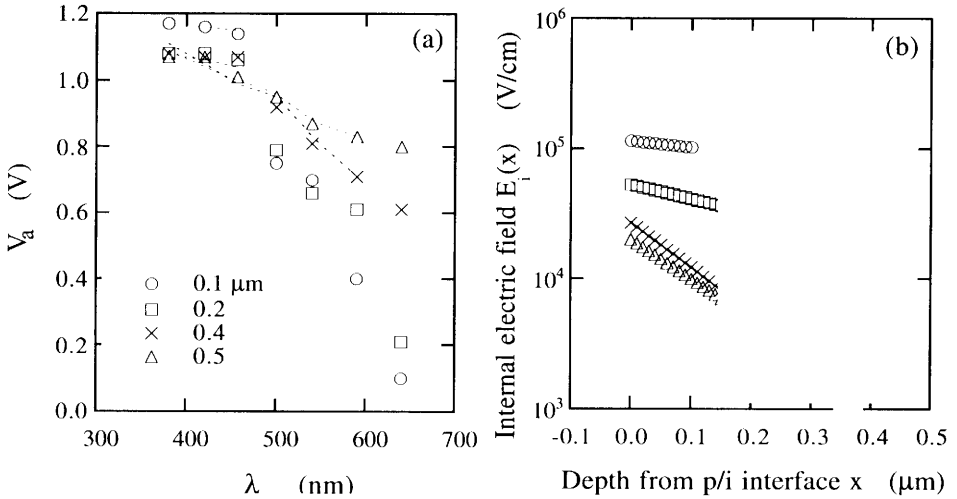


Fig. 1 (a) Applied voltage  $V_a$  vs. the laser wavelength  $\lambda$ , and (b) the  $E_i(x)$  functions used for the best fit, shown by the dotted lines in (a).

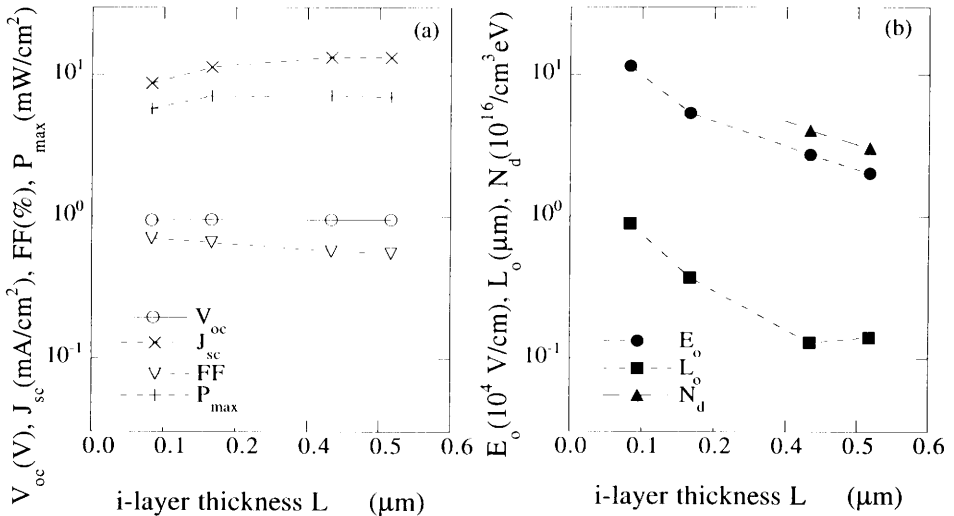


Fig. 2 (a) the cell performance and (b) the internal field parameters as a function of the i-layer thickness.

In Figure 2(a), we plot the cell performance as a function of the i-layer thickness. One can see that  $V_{oc}$  almost does not depend on the i-layer thickness  $L$ , but the short-circuit current  $J_{sc}$  increases with increasing  $L$ . The overall performance  $P_{max}$  increases first and then is saturated when  $L = 0.2 \mu\text{m}$ , because the combination of the increasing of  $J_{sc}$  and the decreasing of the fill factor FF. Figure 2(b) shows the internal electric field parameters as a function of the i-layer thickness  $L$ . Both  $E_o$  and  $L_o$  decrease with increasing  $L$ . Interestingly,  $V_{oc}$  does not depend on the internal field distribution, no matter how much the internal field distribution ( $E_o$  and  $L_o$ ) changes with the i-layer thickness.

### The electric field profile of a-SiGe:H solar cells with varied Ge content

An increased Ge ratio will reduce the band gap of a-SiGe:H materials. We studied the electric field profile of 0.15- $\mu\text{m}$ -thin a-SiGe:H ss/n-i-p/Tco cells with different Ge contents. Figure 3(a) plots the measured  $V_a$  vs.  $\lambda$ . One can see again that  $V_a$  decreases quickly when  $\lambda > 500 \text{ nm}$  in the 0.15- $\mu\text{m}$ -thin cells. We simulated the data for wavelengths less than 500 nm by using the functions in Fig. 3(b). The fits to the data are shown in Fig. 3(a) as the dashed lines. The cell performance, the fitting parameters of  $E_i(x)$  and the deduced defect density  $N_d$  are listed in Table II. We can see that the electric field is stronger for the cell with less Ge content. This is because of a larger optical gap and less defects in the a-SiGe:H i-layer with less Ge content. [8]

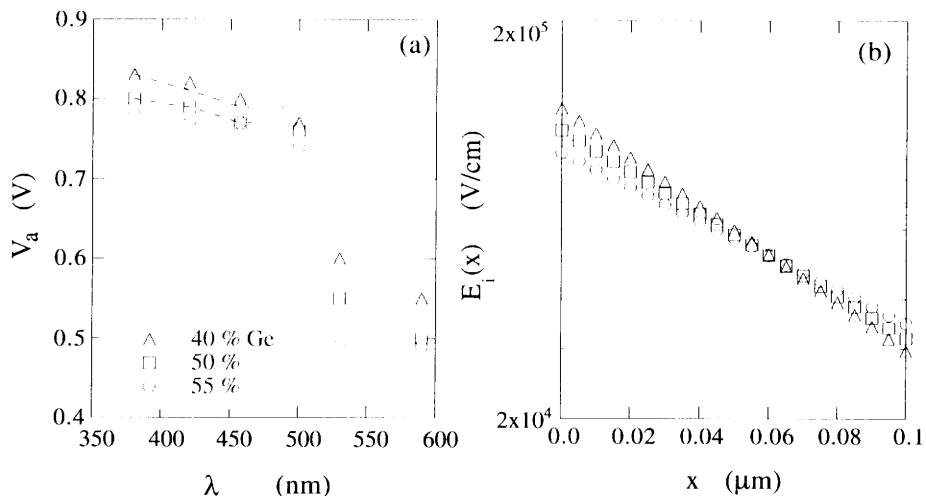


Fig. 3 (a)  $V_a$  vs.  $\lambda$  for the 0.15  $\mu\text{m}$  a-SiGe cells with varied Ge content. The dotted lines are the fits to the data by using the  $E_i(x)$  functions in (b).

Table II. ss/n-i-p/Tco solar cell performance and the fitting parameters of  $E_i(x)$

Sample ID	Ge:Si	$V_{oc}$ (V)	$J_{sc}$ (mA/cm <sup>2</sup> )	FF	$P_{max}$	$E_o$ (V/cm)	$\beta$ ( $\mu\text{m}$ ) <sup>-1</sup>	$L_o$ ( $\mu\text{m}$ )	$N_d$ (cm <sup>3</sup> eV) <sup>-1</sup>
L1	55:45	0.574	14.83	0.540	4.60	$9.31 \times 10^4$	9.886	0.10	$9.7 \times 10^{16}$
L2	50:50	0.673	13.60	0.556	5.09	$1.06 \times 10^5$	12.02	0.083	$1.4 \times 10^{17}$

L3	40:60	0.700	12.01	0.630	5.33	$1.20 \times 10^5$	14.01	0.071	$2.0 \times 10^{17}$
----	-------	-------	-------	-------	------	--------------------	-------	-------	----------------------

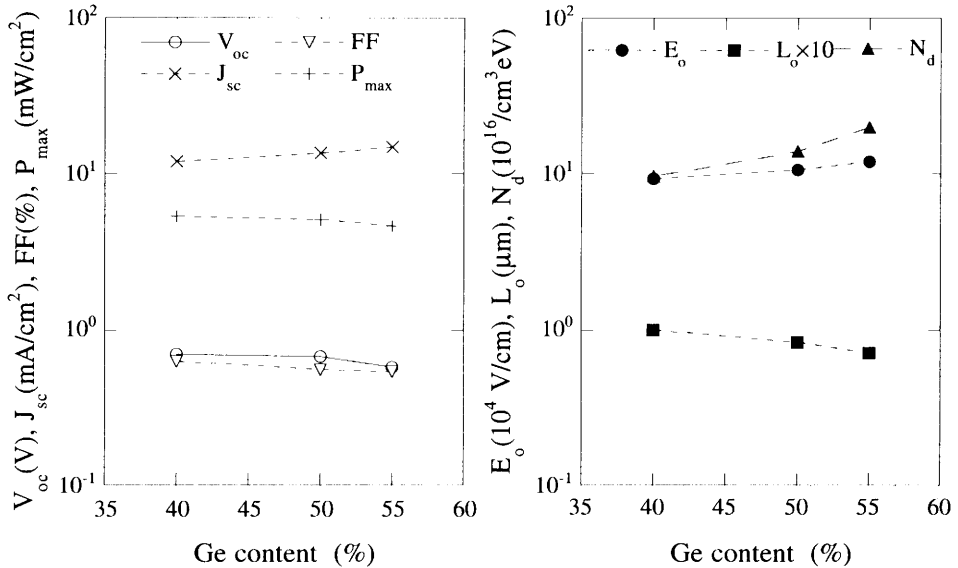


Fig. 4 (a) The cell performance and (b) the internal field parameters as a function of the Ge content in the a-Si-Ge i-layer.

Figure 4 (a) shows the cell performance as a function of the Ge content in the a-Si-Ge:H layer. One can see that  $V_{oc}$ , FF and  $P_{max}$  decrease but  $J_{sc}$  increases with increasing Ge content. Figure 4(b) shows the internal field parameters  $E_0$ ,  $L_0$  and  $N_d$  as a function of the Ge content. Although the values for  $L_0$  and  $N_d$  displayed in figure 4(b) are slightly different for different samples, they are the same within the uncertainty of the fitting technique - one should consider the  $N_d$  values only as an order of magnitude estimate of the defect density. That is because we were only able to use four data points in the fit for each sample, excluding the long-wavelength data as discussed below.

## SUMMARY AND DISCUSSIONS

The null-current method was developed to measure the internal electric field profile for amorphous silicon-based Schottky diode in which only electron transport contributes to the transient photocurrent.[4] The above results testify that the null-current method is also a useful technique to measure the internal electric field profile for a-Si:H p-i-n structures in which both electron and hole transport are involved. The assumption of electron transport domination, and a single exponential function of the internal field,  $E_i(x) = E_0 e^{-\beta x}$ , are valid in a certain wavelength for regions in the sample close to the p/i interface but far from the n/i interface. The assumption of constant defect density is also reasonable near the p/i interface. Therefore, the present technique is available to study the electric field profile in the vicinity of the p/i interface for both p-i-n or n-i-p structures. This region indeed is crucial for solar cell performance. The results of the  $E_i(x)$  profiles are qualitatively consistent with computer simulations.[2,3]

We have studied two groups of solar cells: (a) a-Si:H p-i-n solar cells with varied i-layer thicknesses, and (b) a-SiGe:H cells with varied Ge content. When using an exponential function  $E_i(x) = E_0 e^{-\beta x}$  to fit the experimental results, we obtained the field strength at the p/i interface  $E_0$ ,

the screening length  $L_0$ , and the density of defect states  $N_d$  in the i-layer. From the group (a) samples, our results indicate that for the same quality materials, the thinner the i-layer, the stronger the electric field strength obtained. Whereas  $V_{oc}$  does not change with the i-layer thickness, the internal field profile changes. Both theoretical and experimental studies of the open-circuit voltage,  $V_{oc}$ , of a-Si solar cells have found that the value of  $V_{oc}$  not only depends on the Fermi-level difference of the n- and p-layers, but also on the quality of the p/i interface as well as the i-layer.[9] Especially,  $V_{oc}$  in some devices is dominated by carrier recombination at the p/i junction.[9] The demonstration of an independent value of  $V_{oc}$  on the field profile implies high-quality p/i interfaces in this group of cells. And then both the built-in potential  $E_{bi}$  and the  $V_{oc}$  depend on the Fermi-level difference of the n- and p-layers. An increase in the i-layer thickness results in an increase of  $J_{sc}$  but a decrease of FF. The latter is due to the thicker the i-layer the lower the field strength, consequently the less charge collection. Since the critical electric field strength is  $\xi_c = kT/qL_p$ , for the minority carrier diffusion length  $L_p \approx 0.25 \mu\text{m}$ ,  $\xi_c$  is of the order of  $10^3 \text{ V/cm}$ .[2] As shown in Fig. 1(b),  $E_i(x) > 10^3 \text{ V/cm}$  when  $L < 4000 \text{ \AA}$  which is in agreement with the device design for high performance solar cells. For the group (b) a-SiGe:H cells, the electric field is stronger for the cell with less Ge content. This is because of a larger optical gap in the a-SiGe:H i-layer with less Ge content. [8] One can compare the experimental results of the internal electric field profile with the cell performance as shown in figs. (2) and (4), and then deduce useful information for the device design.

We tend to explain qualitatively the hole limitation as follows. The applied voltage,  $V_a$ , is proportional to the peak value of the transient photocurrent  $j_{pc}$  which corresponds to the collected photocarrier density per second by the internal field  $E_i(x)$ . The photogenerated holes will drift toward the p-side, and the electrons toward the n-side in the internal electric field  $E_i(x)$ . When the short wavelength light illuminates from the p-side, the e-h pairs are generated near the p/i interface due to the shallow absorption depth. The holes will be swiped out through the thin p-layer quickly and the electrons drift oppositely through the i-layer. Since the electron mobility is ten times larger than the hole's, they quickly move through the i-layer. As the wavelength increases, the e-h pairs are generated through the i-layer and then the hole-limitation effect becomes more and more important. When e-h pairs are generated near the n/i interface, the holes must travel through the i-layer with a low mobility that becomes the limitation factor for the photocurrent  $j_{pc}$ . However, the above argument can not explain why the thin cells exhibit a decrease of  $V_a$  at shorter wavelengths. There must be an interface-related reason such as trapped holes near the n/i interface that result in a barrier which depresses the carrier transport. Therefore, one obtains a drastic decrease of  $V_a$  when  $\lambda > 500 \text{ nm}$  as shown in Figs. 1(a) and 3(a) in 0.1 - 0.2  $\mu\text{m}$  thin cells.

## ACKNOWLEDGMENTS

Geng, Wu, and Han are supported by NREL under sub-subcontract XAN-4-13318-09 and XAK-8-17619-11. Deng would like to thank NREL for support under subcontract ZAN-4-13318-11. Wang is supported by DOE subcontract DE-AC02-83CH10093. We are grateful for helpful discussions with Steve Hegedus.

## REFERENCES

1. J. Yang, A. Banerjee, and S. Guha, Amorphous and Microcrystalline Silicon Technology *MRS Symp. Proc.* **467**, edited by M. Hack, E. A. Schiff, R. Schropp, and I. Shimizu, 693 (1997).
2. M. Hack and M. Shur, *J. Appl. Phys.* **58**, 997 and 1656 (1985); **55**, 4413 (1984).
3. J.K. Arch, F.A. Rubinelli, J.-Y. Hou, and S. J. Fonash, *J. Appl. Phys.*, **69**, 7057 (1991).
4. T. Datta and M. Silver, *Appl. Phys. Lett.* **38**, 903 (1981).
5. R. Konenkamp, S Muramatsu, H. Ioth, S. Matsubara, *Appl. Phys. Lett.*, **57**, 478 (1990).
6. R. A. Street, *Phys. Rev B.* **27**, 4924 (1983).
7. Daxing Han, Keda Wang, C.N. Yeh, and Qi Wang, Amorphous and Microcrystalline Silicon Technology, *MRS Symp. Proc.* **467**, edited by M. Hack, E. A. Schiff, R. Schropp, and I. Shimizu, 729 (1997).
8. M. Stutzmann, *J. Appl. Phys.* **66** 569 (1989).
9. S. S. Hegedus, N. Salzman, and E. Fagen, *J. Appl. Phys.* **63**, 5126 (1988).